One-step hydrothermal synthesis of Rare Earth/W-codoped VO_2 nanoparticles: reduced phase transition temperature and improved thermochromic properties

Ning Wang[a], Goh Qing Sheng[a], Lee Pei Lin[a], Shlomo Magdassi[b], Yi Long[a*]

[a] School of Materials Science and Engineering, Nanyang Technological University, 50 Nanyang Avenue, (Singapore) 639798

[b] Institute of Chemistry, Edmund Safra Campus, The Hebrew University, Jerusalem 91904, Israel.

[*]Corresponding author: Dr Long Yi, tel.: (65) 67904599, Fax: (65) 67911604, E-mail: longyi@ntu.edu.sg

Abstract. As a reversible thermochromic material, vanadium dioxide (VO_2) is a promising candidate for smart window applications. The trade-off between the integrated visible transmission (T_{lum}) and the solar modulating ability (ΔT_{sol}), as well as the high phase transition temperature (τ_c~68 °C) are regarded as the main obstacles for practical applications of pure VO_2 nanomaterials. The combination of both high τ_c reducing efficiency of W and improving $T_{lum}/\Delta T_{sol}$ properties of RE (rare earth: Eu, Tb), herein lies the purpose of RE/W-codoping to enhance the thermochromic performance. The RE/W-codoped VO_2 nanoparticles were synthesized under hydrothermal conditions, and exhibited grain size of less than 100 nm. The smart window which was fabricated by coating RE/W-codoped VO_2 nanoparticles onto glass, exhibits a thermochromic performance with a combination T_{lum}= 40%, ΔT_{sol}= 6.3%, τ_c= 40.8 °C or T_{lum}= 63%, ΔT_{sol}= 3.6%, τ_c= 31.9 °C, indicating the largely reduced absorption compared with the single W doping. Under the RE/W-codoping conditions, it was found that the ionic radius of the RE^{3+} cations controlled the crystallinity of the VO_2 particles and the electron/hole carrier counteraction as well as the competition between the strain and the hole carrier played a vital role in modulating the τ_c of the VO_2 products. The findings should be meaningful for investigating the codoping mechanisms for VO_2 nanomaterials.

Keywords. Vanadium dioxide; Solar modulation; Hydrothermal synthesis; Thermochromic smart window; Doping.

1. Introduction

Vanadium dioxide (VO_2) is a well-known thermochromic material, exhibiting a solar modulating ability across its phase transition temperature (τ_c≈68 °C), i.e. the high transmission and the high absorption/reflection could be obtained below and above the τ_c, respectively [1-7]. In light of the solar modulating ability, VO_2 has been intensely investigated for applications in smart

window. It permits the transmission of visible and IR light below τ_c, and selectively blocks the IR radiation above the τ_c, thus maintaining a comfortable in-door temperature [8-10]. However, the requirements for practical applications of the smart window (high visible transmission (T_{lum}>70%), large solar modulating ability (ΔT_{sol}>10%), near ambient τ_c, etc.) are difficult to achieve for normal VO_2 materials, due to a trade-off between the T_{lum} and the ΔT_{sol}, and the high τ_c which is far off from 25 °C [11-13].

As for the thermochromic performance, the high T_{lum} is to get the clear vision while the large ΔT_{sol} is to promise the enough energy saving efficiency. In order to improve the thermochromic performance of VO_2 nanomaterials, several techniques have been applied to modify the physical and/or chemical characteristics of VO_2 nanomaterials. This includes the porous assembly [14-17], nanocomposite [18-22], patterning [11, 23, 24], antireflection coating [25, 26] as well as the doping[3, 27]. Among these techniques, doping is an easy-to-control and cost-effective choice for tailoring the thermochromic properties of VO_2. As reported in literatures, doping by the cations with the valence state larger than 4+ and/or with the ionic radius larger than 0.58 Å could reduce the τ_c [28]. On the other hand, doping by the cations with the valence state less than 4+ or with the ionic radius smaller than 0.58 Å could be used to increase the τ_c [28]. Notably, the W^{6+} doping was reported to show the highest experimental τ_c reducing rate 20-26 °C/at% [29-31]. With respect to the integrated visible transmittance (T_{lum}) and the integrated solar modulating ability (ΔT_{sol}), Mg doping was found to be able to improve the T_{lum} by widening the band gap of VO_2(M) at a rate of 3.9 eV/at.% [32], the Zr doping could enhance the T_{lum} by a relative percentage of 65%[33] and the RE (rare earth: Eu, Tb, La) doping[34-36] has the ability to increase the T_{lum} and the ΔT_{sol} simultaneously. However, it is challenging to obtain a largely reduced τ_c and improved T_{lum} as well as ΔT_{sol} concurrently through single doping. In recent studies, it was reported that Mg/W-codoping could exhibit low τ_c and enhanced T_{lum}/ ΔT_{sol} by

combining the advantages of Mg and W doping in T_{lum} increasing and τ_c reducing respectively [37] and W/F-codoped VO_2 thin films could also show the reduced τ_c and improved visible transmittance [43]. Besides, the Cr/Nb-codoping was reported to be helpful in achieving the large TCR (temperature coefficient of resistance) with no thermal hysteresis [44]. Therefore, codoping may be a promising approach to optimize the thermochromic performance of VO_2 smart windows.

In this paper, the RE/W-codoping is proposed for the first time to enhance the thermochromic performance of VO_2 by utilizing the large τ_c reducing ability of W and the $T_{lum}/\Delta T_{sol}$ increasing capability of RE. The RE/W-codoped VO_2 nanoparticles were hydrothermally assembled to fabricate the thin film smart windows, which were expected to show a low τ_c and improved T_{lum} as well as ΔT_{sol}. The possible mechanism for the RE/W-codoping effect is also discussed in detail.

2. Materials and methods

All chemicals used in this paper, V_2O_5 (Alfa Aesar, 99.6%), Tb_2O_3 (Alfa Aesar, 99%), Eu_2O_3 (Alfa Aesar, 99%), H_2WO_4 (Alfa Aesar, 99.6%), H_2O_2 (Sigma-Aldrich), polyvinylpyrrolidone (PVP, 99%, Sigma-Aldrich) and $N_2H_4{\cdot}H_2O$ (Alfa Aesar, 99.9%) were used as received without any further purification.

Hydrothermal synthesis of RE/W-codoped VO_2 nanopowders. 5 mL 30 wt% H_2O_2 solution was preheated at 90 °C for 3 min in a 300 mL glass beaker. 233 mg V_2O_5, 6.4 mg H_2WO_4 and weighed Tb_2O_3/Eu_2O_3 powders based on the Eu/Tb doping level 1-6 at% were then added into the hot H_2O_2 solution. After a vigorous evaporation, the yellowish precursor was chemically reduced by 45 μL $N_2H_4{\cdot}H_2O$. It was then transferred and sealed into a 50 mL stainless-steel autoclave with a Teflon liner. After heating at 260 °C for 24h in an oven and then cooling to room temperature in

the air, the products were collected by centrifuging (10000 rpm) 3 times with 10 mL acetone and drying overnight in a vacuum oven.

Fabrication of thin films. 50 mg of RE/W-codoped VO_2 nanoparticles were dispersed in 15 mL of ethanol with ultrasonic irradiation for 10 min. Thereafter 40 mg of PVP was further added into the dispersion to improve the dispersion viscosity and stirred for 5 min. The obtained brown-colored VO_2 dispersion was then knife casted onto glass substrate to get the thin film. An additional annealing at 400 °C for 1h in Ar atmosphere was ultimately applied to increase the adhesion and the film crystallinity. The sample names (0Eu0W-3Tb1W) under different RE/W atomic doping levels have been clarified in Table 1.

Characterization. The XRD characterization was performed with a Shimadzu XRD-6000 X-ray diffractometer (Cu-Kα, λ = 0.15406 nm) with a voltage 40 kV and a current 30 mA. Raman spectra were recorded with the Confocal Raman Witec alpha300 SR under 785 nm laser at room temperature. The morphology of the products was characterized using a field emission scanning electron microscope (FESEM, JSM-7600F, JEOL, Japan) at an accelerating voltage 5 kV and a probe current 7 μA. The morphology and the crystalline phase were further measured with the transmission electron microscopy (TEM, JEOL-2010, JEOL, Japan) at an accelerating voltage of 200 kV. The elemental analysis of the product were carried out using the EDX equipped on the FESEM and TEM. The phase transition temperature of the codoped VO_2 products was determined with a differential scanning calorimeter (DSC Q10, TA Instruments, USA), and the DSC data were collected in the temperature range 5-60 °C under a N_2 atmosphere. The film thickness and the optical constants were measured with VASE Ellipsometer (VB-400, J.A. Woollam Co., Inc. USA). The UV-Vis-NIR transmittance spectra (250 nm<λ<2500 nm) were recorded using a UV-Vis-NIR spectrophotometer (Cary 5000, Agilent Ltd, USA) equipped with a

Linkam PE120 system Peltier heating & cooling stage. The integrated visible transmittance (T_{lum}, 380 nm<λ<780 nm) and solar transmittance (T_{sol}, 280 nm<λ<2500 nm) were calculated based on the expression

$$T_{lum/sol}=\int\varphi_{lum/sol}(\lambda)T(\lambda)d\lambda/\int\varphi_{lum/sol}(\lambda)\,d\lambda \quad (1)$$

where $T(\lambda)$ is the recorded %T, φ_{lum} is the standard luminous efficiency function for the photopic vision of human eyes[38] and φ_{sol} is the solar irradiance spectrum for air mass 1.5 (corresponding to the sun standing 37˚ above the horizon) [39]. ΔT_{sol} is calculated as $\Delta T_{sol}=T_{sol}(\tau<\tau_c)- T_{sol}(\tau>\tau_c)$.

3. Results and discussion

3.1 Synthesis of RE/W-codoped VO_2 nanoparticles

Figure 1 shows the XRD patterns of the RE/W-codoped VO_2 nanoparticles, synthesized hydrothermally. The corresponding formula of the samples 0Eu0W (pure VO_2)-6Eu1W (VO_2 doped with 6 at% Eu and 1 at% W), 1Tb0W-3Tb1W with different RE/W doping levels has been tabulated in Table 1. The Eu/Tb/W doping levels in the VO_2 samples have also been determined by the EDX in terms of Eu (at%)/V(at%), Tb (at%)/V(at%) and W (at%)/V(at%). As shown in Figure 1A, the XRD pattern of the sample 0Eu0W shows the major VO_2(M) phase (JCPDS #82-661), and the additional peak at ~27° (2θ) should be attributed to the V_6O_{13} impurity. Interestingly, the XRD pattern of the sample 0Eu1W shows the pure VO_2(M) phase with the crystalline planes (011), (-102), (-211), (020), (-212), (220) and (002), indicating that the tungsten dopant may help to promote the crystallization of VO_2(M). As for the samples 1Eu1W-6Eu1W, an additional $EuVO_4$ phase (JCPDS #15-0809) with the faces (101), (200), (220), (103), (312) and (400) could be

indexed in the XRD pattern. Whereas for the Tb/W-codoped VO_2, as shown in Figure 1B, the samples 1Tb0W-3Tb1W exhibit the combination of VO_2 (M) phase and the $TbVO_4$ (JCPDS #17-0340) impurity in the corresponding XRD patterns. The XRD result reveals that the VO_2(M) phase can be successfully attained under the RE/W-codoping hydrothermal conditions, but the impurity ($TbVO_4$, $EuVO_4$) is difficult to be eliminated, which may be due to the high affinity of RE to V in the chemical reaction and/or the extremely low solubility of RE oxides. The phase composition of the pristine VO_2 (0Eu0W) was also confirmed by the Raman spectra (Figure 1C), where the peaks at 146 (A_g), 196 (A_g), 226 (A_g), 288 (A_g), 403 (A_g), and 485 (A_g) cm^{-1} could be assigned to the V-O vibration of the monoclinic VO_2 (M) phase, and the peaks at 166, 266 cm^{-1} should be attributed to the V_6O_{13} impurity.

The obtained RE/W-codoped VO_2 nanoparticles were further characterized with TEM. As depicted in Figure 2A-P, all the undoped (0Eu0W, Figure 2A, B) and Eu/W-codoped (0Eu0W-6Eu1W, Figure 2C-P) VO_2 samples show the morphology of nanoparticles with the size below 100 nm. The VO_2 (M) phase was further confirmed by the SAED patterns (inset in Figure 2) and the HRTEM images (Figure 2B, D, F, H, I, L, N, P) which can be indexed with the standard VO_2 (M) crystalline faces (011), (-211) and (200). In addition, the $EuVO_4$ impurity could also be indexed in the SAED patterns of the Eu/W-codoped samples. The V/Eu/W elemental mapping for the sample 5Eu1W was performed representatively to identify the dopant distribution in the nanoparticles. As shown in Figure 2Q, the signal of Eu-Lα and W- Lα in the VO_2 nanoparticles where V-Kα populated is distributed continuously, revealing the efficient Eu/W doping for the sample. Due to the disturbance of $EuVO_4$ impurity, the unexpected concentrated Eu-Lα signal at the impurity position could be pointed out in the mapping. Similarly, the morphology and the crystalline phase of the Tb/W-codoped VO_2 nanoparticles were also validated in the TEM images as shown in Figure 3. The VO_2(M) crystalline phase could be easily indexed in the HRTEM images

(Figure 3B, D, F, H, J, L, N) and the $TbVO_4$ impurity could be figured out in the corresponding SAED patterns (inset figure). The continuous Tb/W-codoping was also observed in the V/Tb/W elemental mapping for the sample 3Tb1W as illustrated in Figure 3O. Due to the impurity of $TbVO_4$/$EuVO_4$ in the products, the doping level of the RE/W-codoped VO_2 were roughly determined using the EDX equipped in the TEM by focusing on the selected pure phase VO_2 nanoparticles (Table 1).

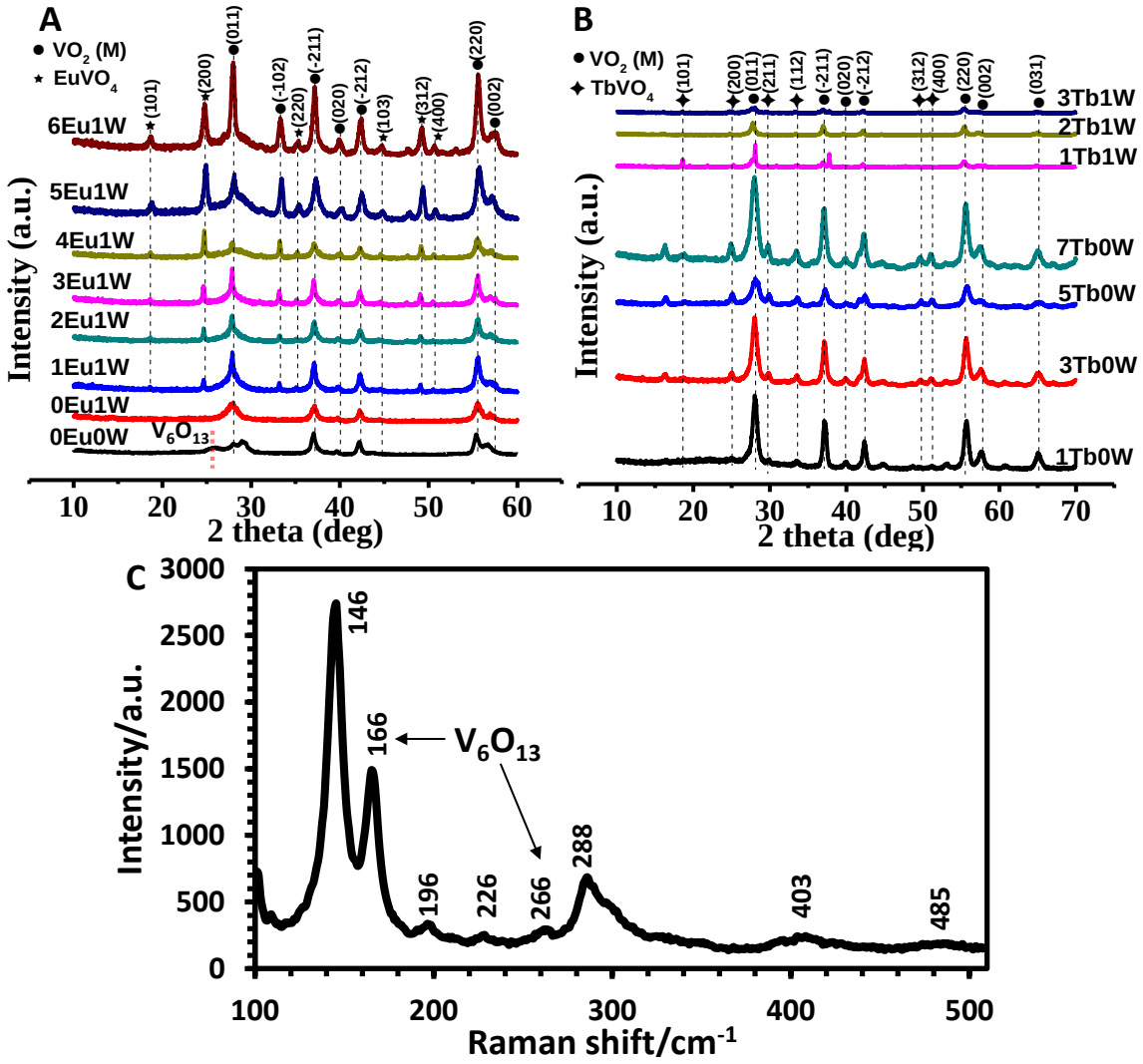

Figure 1 XRD patterns of the Eu/W codoped (A) and Tb/W-codoped VO_2 nanopowders (B). (C) Raman spectra of the pristine VO_2 sample (0Eu0W). Laser wavelength=785 nm.

3.2 Phase transition of RE/W-codoped VO_2 nanoparticles

Figure 4 shows the phase transition of the RE/W-codoped VO_2 nanopowders determined by DSC cycling measurement. Due to the low crystallinity of as-prepared products, the Eu/W-codoped VO_2 nanoparticles were tested after an additional annealing at 400 °C for 1h in Ar flow. As shown in Figure 4A and Table 1, to begin with 1 at% W doping (0Eu1W), the phase transition temperature τ_c could be decreased from the pristine 61.7 °C (0Eu0W) to 42°C in accordance with the reported τ_c reducing efficiency of W doping [29]. Upon increasing the Eu doping level from 0 (0Eu1W) to 1 (1Eu1W) and 2at% (2Eu1W), the τ_c was slightly increased from 42 to 46.7 and 49.2 °C, respectively, mainly owing to the neutralization of free electron carrier from the W^{6+} doping by the introduced hole carrier from the Eu^{3+} doping. However, upon increasing the doping level of Eu to 3 at% (3Eu1W) and 4 at% (4Eu1W), the τ_c began to decrease to 48.6 and the minimum 38.1 °C, respectively, which indicates the dominant role of the extra strain from the lattice distortion of Eu/W-codoped VO_2 under both the doping levels. With further increasing the Eu doping level to 5 at% (5Eu1W) and 6 at% (6Eu1W), the largely increased hole carrier density from Eu^{3+} doping started to control the τ_c modulation, which resulted in the slight increase of τ_c to 47.2 and 48.2 °C, respectively. However, the τ_c reduction by hole carriers incorporated into the $d_{\|}$ sub-bands has been reported by *Zhang* et al. [46]. Therefore, the increase of τ_c by hole carriers in the Eu^{3+} highly doping conditions should be due to the incorporation of hole carriers into the $d_{\|}^*$ or π^* sub-bands, which will be confirmed by the future studies. With respect to the Tb/W-codoped VO_2 nanoparticles, as shown in Figure 4B and Table 1, the single Tb doping (1Tb0W-7Tb0W) could reduce the τ_c from 61.7 °C of pristine VO_2 (0Eu0W) to around 50 °C at the single Tb doping level of 5 at%. Under Tb/W-codoping conditions, upon increasing the Tb doping level from 1 (1Tb1W), 2 at% (2Tb1W) to 3 at% (3Tb1W), the τ_c had steadily decreased to 40.8, 36.5 and 31.9 °C respectively, mainly ascribed to the extra strain

arising from the Tb doping in the lattice. Moreover, the latent heat of phase transition for the sample 1Tb0W can reach 35.83 J/g, which is comparable to the value 41.87 J/g for commercial VO_2 product (Alfa-Aesar)[40], revealing the high crystallinity of the product. Even at the Tb/W-codoping conditions, the phase transition latent heat could also remain 12.51 J/g for 1Tb1W, 15.93 J/g for 2Tb1W and 5.81 J/g for 3Tb1W. The higher crystallinity of Tb doped VO_2 than that of Eu doped ones should be due to the smaller ionic radius of Tb^{3+} (0.92 Å) than that of Eu^{3+} (0.95 Å), since the crystallinity could be reduced by the significant deformation of the lattice.

3.3 Thermochromic properties

Figure 5A shows the UV-Vis-NIR transmittance spectra of the RE/W-codoped VO_2 thin films prepared by casting powder products onto glass substrates. All the VO_2 thin films show the solar modulations across the cold (20 °C) and hot (90 °C) conditions in the near infrared (NIR) region. The %T contrast at the wavelength 2500 nm could be increased from 37.5% for pristine VO_2 (0Eu0W) to 37.8% and 38.5% when the VO_2 was doped with Eu/W (2Eu1W) and Tb/W (1Tb1W), respectively. Moreover, the Tb/W-codoping (1Tb1W, 2Tb1W, 3Tb1W) was found to be able to improve the visible transmission by 100% or higher compared with the pristine VO_2. The integrated visible transmission (T_{lum}) and the solar modulating ability (ΔT_{sol}) for the RE/W codoped VO_2 thin films were calculated based on the %T spectra, and have been tabulated in Table 1. As depicted in Table 1, the pristine VO_2 (0Eu0W) showed the largest ΔT_{sol}=7.3% and a low T_{lum}(20/90 °C)=20.3%/21.2%. With single 1 at% W doping, the annealed sample 0Eu1W showed an increased T_{lum}(20/90 °C)=50.4%/52.5% and a largely reduced ΔT_{sol}=2.8%. With Eu/W-codoping, the annealed 5Eu1W and 2Eu1W could recover the ΔT_{sol} to 4.6% and 5.2% respectively, but the T_{lum}(20/90 °C) was largely reduced to corresponding 15.2%/18.1% and 16.5/18.6%. Comparatively, the Tb/W-codoping (1Tb1W, 2Tb1W, 3Tb1W) was found to be effective in

enhancing the T_{lum} and increasing the ΔT_{sol}. For the sample 1Tb1W, the ΔT_{sol} could be recovered to 6.3%, nearly 90% of the pristine VO_2, and the T_{lum}(20/90 °C) was increased to 37.5%/43.1%, which is ~2 times larger than that of the pristine VO_2. As for the sample 3Tb1W, the T_{lum} was further increased to 60.9%/65.0%, almost 3 times larger than that of the pristine VO_2, but the ΔT_{sol} was reduced to 3.6%. Although the thermochromic properties cannot reach the best reported values for the VO_2 nanoparticles (T_{lum} =~50%, ΔT_{sol}=~20%)[41], this first investigation on the RE/W-codoping should be meaningful for maintaining proper thermochromic performance when reducing the τ_c to near room temperature, and should be useful for studying the doping mechanism in VO_2 materials.

In order to further investigate the RE/W-codoping effects, the optical band gap (Eg) was determined by fitting the linear part of the curve $(\alpha\hbar\omega)^2$ v.s. $\hbar\omega$ (Figure 5B) according to the expression

$$(\alpha\hbar\omega)^2=A(\hbar\omega-Eg) \quad (2)$$

Where α is the absorption coefficient [αd=-ln(T/1-R)], A is a constant and $\hbar\omega$ is the photon energy ($\hbar\omega/eV = \frac{1240}{\lambda/nm}$). As seen in Figure 5B, the annealed single W-doped VO_2 (0Eu1W) showed an increase of band gap (Eg=2.50 eV) compared with the annealed pristine VO_2 (0Eu0W, Eg=2.33 eV) which should attribute to the increase of the T_{lum}, and is not consistent with the band gap narrowing effect of the W doping[42]. This should be due to the reduction of the lattice distortion arising from the W doping during the annealing process [41], since the lattice distortion is proportional to the band gap narrowing, and the band gap widening could give rise to the increase of T_{lum}. As for the as-prepared Tb/W-codoping (1Tb1W, 2Tb1W, 3Tb1W), Eg was gradually increased from 2.24 to 2.30 eV along with the continuous Tb doping, in accordance with the band gap widening effect of RE doping[34], which also gave rise to the increase of T_{lum}

as described above. The Eg of the as-prepared Tb/W-codoped VO_2 is slightly lower than the pristine VO_2, which should be due to the band gap narrowing effect of the W doping [42].

The complex refractive index (N=n+ik) for the RE/W codoped VO_2 was also determined using ellipsometry. As shown in Figure 6B, comparing with the pristine VO_2 (0Eu0W), the refractive index (*n*) of 2Tb1W was evidently reduced above 600 nm, which should contribute to the largely enhanced T_{lum} as indicated in Table 1 and Figure 6A. The 2Eu1W did not show apparent changes of the refractive index compared with 0Eu0W, which indicated the weak T_{lum} modulation, in accordance with the %T measurement in Table 1. Based on the Ravindra relation [45], the band gap could be expressed as N=4.16-0.85 Eg, where $N=(n^2+k^2)^{1/2}$. According to the Eg expression, the calculated Eg (λ=1290 nm) for the samples 0Eu0W, 2Eu1W and 2Tb1W is 2.39 eV, 2.41 eV and 2.40 eV, respectively, which is similar to the value fitted from the UV-Vis-NIR spectra, further proving the RE/W-codoping effect on the Eg of VO_2.

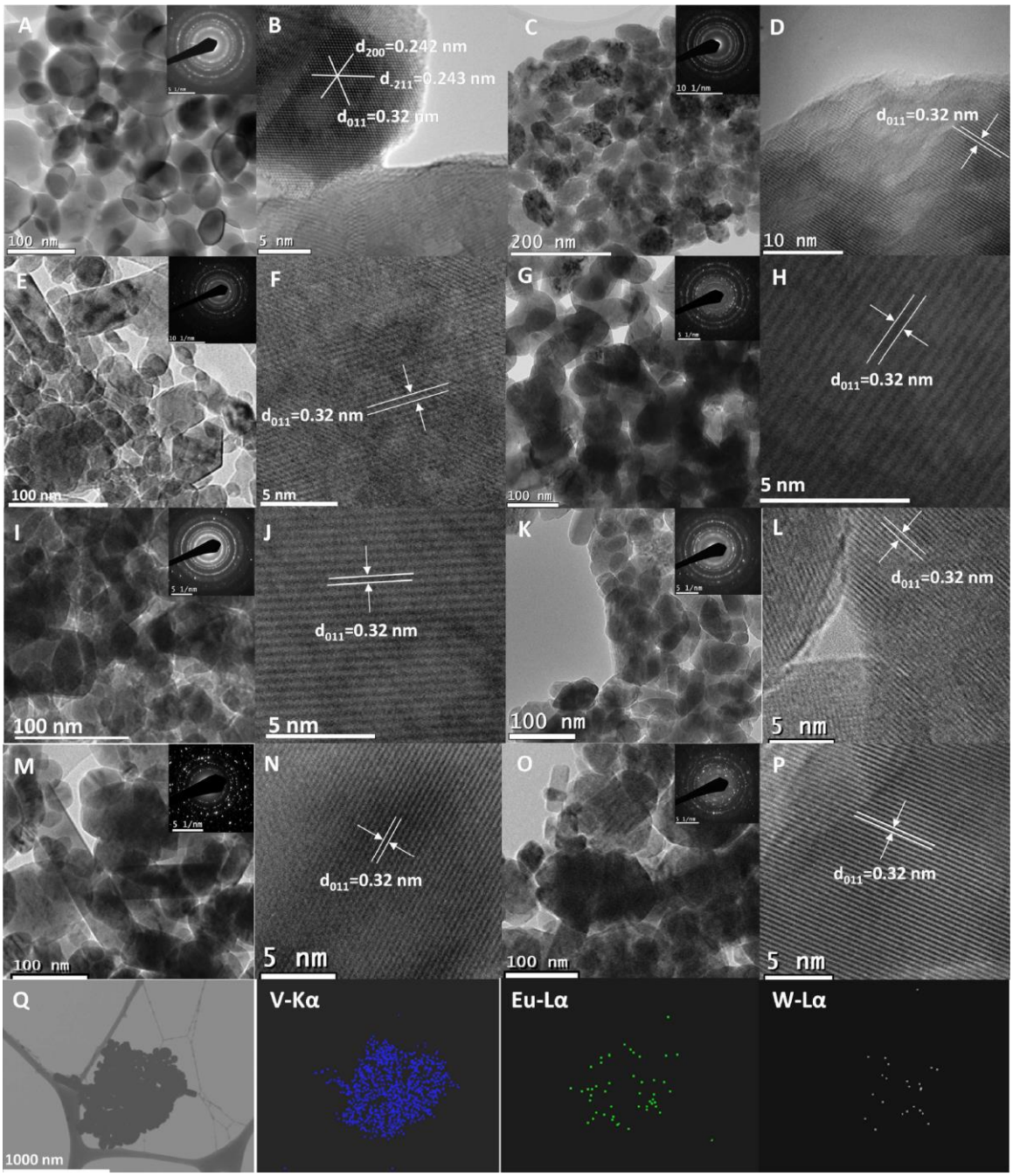

Figure 2 Bright-field TEM images (A, C, E, G, I, K, M, O) and the corresponding SAED patterns (inset) as well as the HRTEM images (B, D, F, H, J, L, N, P) for the samples 0Eu0W (VO_2, A, B), 0Eu1W ($V_{0.99}W_{0.01}O_2$, C, D), 1Eu1W ($V_{0.98}Eu_{0.01}W_{0.01}O_2$, E, F), 2Eu1W ($V_{0.97}Eu_{0.02}W_{0.01}O_2$, G, H), 3Eu1W ($V_{0.96}Eu_{0.03}W_{0.01}O_2$, I, J), 4Eu1W ($V_{0.95}Eu_{0.04}W_{0.01}O_2$, K, L), 5Eu1W ($V_{0.94}Eu_{0.05}W_{0.01}O_2$, M,

N) and 6Eu1W ($V_{0.93}$ $Eu_{0.06}W_{0.01}O_2$, O, P) nanoparticles. (Q) FESEM image and the corresponding V-Kα, Eu-Lα and W-Lα elemental mapping of the 5Eu1W nanoparticles.

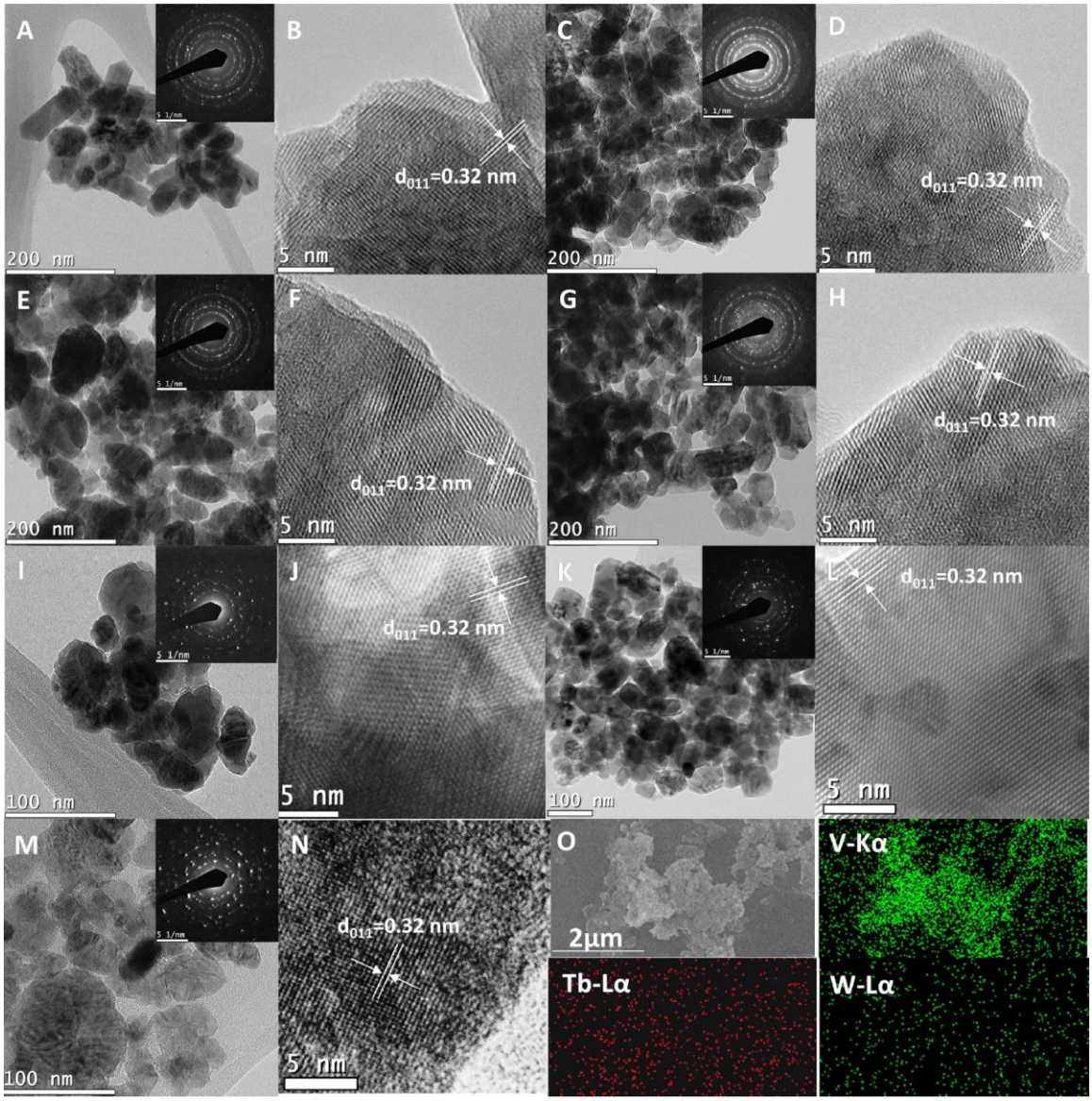

Figure 3 Bright-field TEM images (A, C, E, G, I, K, M) and the corresponding SAED patterns (inset) as well as the HRTEM images (B, D, F, H, J, L, N) for the samples 1Tb0W ($V_{0.99}Tb_{0.01}O_2$, A, B), 3Tb0W ($V_{0.97}Tb_{0.03}O_2$, C, D), 5Tb0W ($V_{0.95}Tb_{0.05}O_2$, E, F), 7Tb0W ($V_{0.93}Tb_{0.07}O_2$, G, H), 1Tb1W ($V_{0.98}Tb_{0.01}W_{0.01}O_2$, I, J), 2Tb1W ($V_{0.97}Tb_{0.02}W_{0.01}O_2$, K, L) and 3Tb1W ($V_{0.96}Tb_{0.03}W_{0.01}O_2$, M, N)

nanoparticles. (O) FESEM image and the corresponding V-Kα, Tb-Lα and W-Lα elemental mapping of the 3Tb1W nanoparticles.

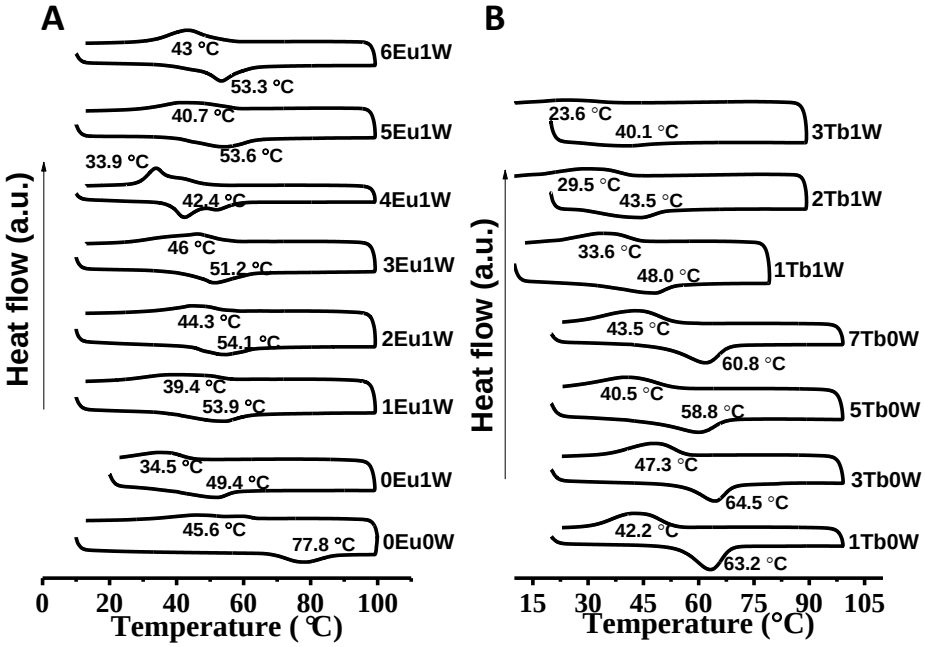

Figure 4 Heating and cooling DSC cycles for the RE/W-codoped VO_2 nanoparticles. (A) Eu/W-codoped VO_2 with additional annealing at 400 °C for 1 h. (B) As-prepared Tb/W-codoped VO_2.

Table 1 Thermochromic properties of the RE/W-codoped VO_2 nanoparticles.

Sample	Formula	Doping level/at%		τ_c/ °C[b]	d[c]/nm	T_{lum}(20/90 °C)/%	ΔT_{sol}/%[d]
		Expected	EDX[a]				
0Eu0W	VO_2	-	-	61.7	62	20.3/21.2	7.3
0Eu1W	$V_{0.99}W_{0.01}O_2$	W:1	0.9	42.0	57	50.4/52.5	2.8
1Eu1W	$V_{0.98}Eu_{0.01}W_{0.01}O_2$	Eu:1/W:1	Eu:0.9/W:0.7	46.7	60	25.3/28.4	2.0

2Eu1W	$V_{0.97}Eu_{0.02}W_{0.01}O_2$	Eu:2/W:1	Eu:1.7/W:0.9	49.2	63	16.5/18.6	5.2
3Eu1W	$V_{0.96}Eu_{0.03}W_{0.01}O_2$	Eu:3/W:1	Eu:2.9/W:1.3	48.6	77	26.5/28.5	2.1
4Eu1W	$V_{0.95}Eu_{0.04}W_{0.01}O_2$	Eu:4/W:1	Eu:3.7/W:1.1	38.1	49	12.3/9.6	2.4
5Eu1W	$V_{0.94}Eu_{0.05}W_{0.01}O_2$	Eu:5/W:1	Eu:5.6/W:1.2	47.2	53	15.2/18.1	4.6
6Eu1W	$V_{0.93}Eu_{0.06}W_{0.01}O_2$	Eu:6/W:1	Eu:5.3/W:0.7	48.2	68	31.4/34.5	-1.3
1Tb0W	$V_{0.99}Tb_{0.01}O_2$	Tb:1	Tb:1.5	52.7	80	69.3/71.9	1.9
3Tb0W	$V_{0.97}Tb_{0.03}O_2$	Tb:3	Tb:3.3	55.9	78	78.1/78.6	2.1
5Tb0W	$V_{0.95}Tb_{0.05}O_2$	Tb:5	Tb:4.7	49.7	49	53.4/54.5	0.8
7Tb0W	$V_{0.93}Tb_{0.07}O_2$	Tb:7	Tb:6.7	52.2	42	65.6/68.6	2.0
1Tb1W	$V_{0.98}Tb_{0.01}W_{0.01}O_2$	Tb:1/W:1	Tb:0.8/W:0.9	40.8	73	37.5/43.1	6.3
2Tb1W	$V_{0.97}Tb_{0.02}W_{0.01}O_2$	Tb:2/W:1	Tb:1.9/W:0.8	36.5	69	54.7/59.7	4.7
3Tb1W	$V_{0.96}Tb_{0.03}W_{0.01}O_2$	Tb:3/W:1	Tb:3.1/W:1.1	31.9	45	60.9/65.0	3.6

Note: [a]EDX derivation is ±10%, [b]$\tau_c=(\tau_{c,cool}+\tau_{c,heat})/2$, [c] *d* is the film thickness, [d]$\Delta T_{sol}=T_{sol}(20\ °C)-T_{sol}(90\ °C)$

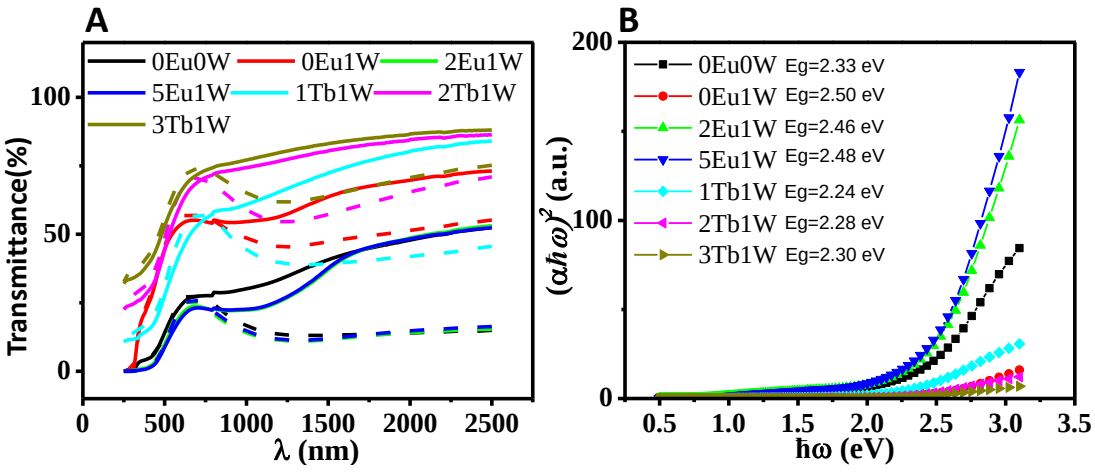

Figure 5 (A) UV-Vis-NIR %T spectra of the annealed 0Eu0W, 0Eu1W, 2Eu1W, 5Eu1W and the as-prepared 1Tb1W, 2Tb1W and 3Tb1W recorded at 20 °C (solid lines) and 90 °C (dash lines), respectively. (B) Corresponding plots of $(\alpha\hbar\omega)^2$ v.s. $\hbar\omega$, where the optical band gap Eg was determined by fitting the linear part of the curves.

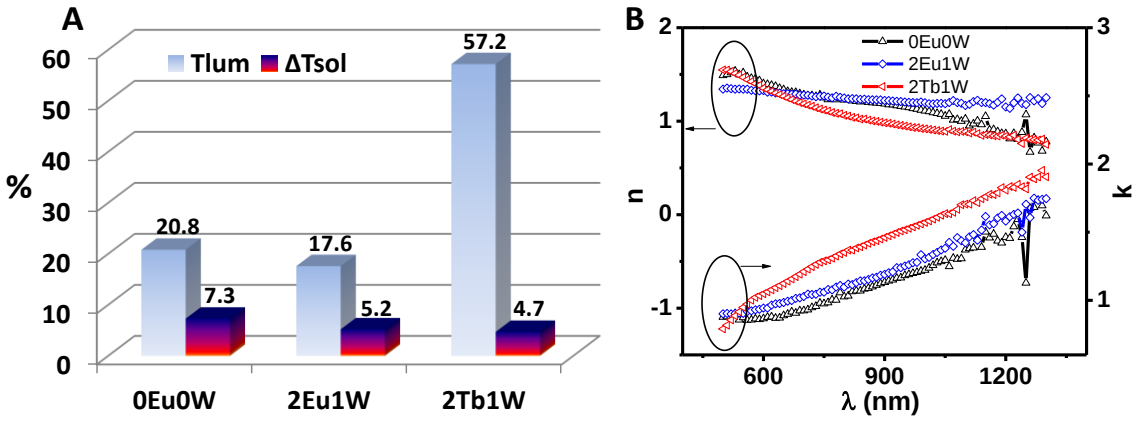

Figure 6 (A) Averaged T_{lum} and ΔT_{sol} for the annealed 0Eu1W, 2Eu1W and the as-prepared 2Tb1W samples. (B) Corresponding refractive index '*n*' and the extinction coefficient '*k*' tested at room temperature by ellipsometer.

Conclusion

In summary, the effect of RE/W-codoping on modulating the thermochromic properties of VO_2 nanomaterials was investigated for the first time. The Eu/W- and Tb/W-codoped VO_2 nanoparticles were one-step synthesized by a simple hydrothermal process. Due to the larger ionic radius of Eu^{3+}, the obtained Eu/W-codoped VO_2 nanoparticles exhibited less crystallinity than the Tb/W-codoped VO_2 nanoparticles, which can then be overcome by an additional annealing process. Both the annealed Eu/W- and as-prepared Tb/W-codoped VO_2 nanoparticles exhibited reduced τ_c and proper combination of T_{lum} and ΔT_{sol}. The Tb/W-codoping was found to

be effective in improving both the T_{lum} and ΔT_{sol} as compared with single W doping, which provides an alternative approach for enhancing thermochromic properties and reducing τ_c to ambient temperature. Overall, the hydrothermal synthesized RE/W-codoped VO_2 nanoparticles successfully overcame the limit of T_{lum} and ΔT_{sol} for single W-doping, which should be of great importance for the practical applications of VO_2 in smart windows, and should be meaningful for investigating the codoping mechanisms.

Acknowledgments

This research is supported by the National Research Foundation, Prime Minister's Office, Singapore under its Campus for Research Excellence and Technological Enterprise (CREATE) programme, Singapore Ministry of Education (MOE) Academic Research Fund Tier 1 RG101/13, and JTC-sponsored FYP program AY 2016-17. XRD, FESEM and TEM characterization was performed at the Facility for Analysis, Characterization, Testing and Simulation (FACTS) in Nanyang Technological University, Singapore. The authors Goh Qing Sheng and Lee Pei Lin thank the NTU-JTC Industrial Infrastructure Innovation Centre Singapore for their support.

[1] F. Morin, Oxides Which Show a Metal-to-Insulator Transition at the Neel Temperature, Phys. Rev. Lett. 3 (1959) 34-36.

[2] M.M. Seyfouri, R. Binions, Sol-gel approaches to thermochromic vanadium dioxide coating for smart glazing application, Sol. Energy Mater. Sol. Cells 159 (2017) 52-65.

[3] S. Wang, M. Liu, L. Kong, Y. Long, X. Jiang, A. Yu, Recent progress in VO_2 smart coatings: Strategies to improve the thermochromic properties, Prog. Mater Sci. 81 (2016) 1-54.

[4] M.E.A. Warwick, R. Binions, Advances in thermochromic vanadium dioxide films, J. Mater. Chem. A 2 (2014) 3275-3292.

[5] V. Eyert, The metal-insulator transitions of VO_2: A band theoretical approach, Annalen der Physik 11 (2002) 650-704.

[6] M.F. Becker, A.B. Buckman, R.M. Walser, T. Lépine, P. Georges, A. Brun, Femtosecond laser excitation dynamics of the semiconductor-metal phase transition in VO_2, J. Appl. Phys. 79 (1996) 2404-2408.

[7] R. Heckingbottom, J.W. Linnett, Structure of Vanadium Dioxide, Nature 194 (1962) 678-678.

[8] Y. Gao, H. Luo, Z. Zhang, L. Kang, Z. Chen, J. Du, M. Kanehira, C. Cao, Nanoceramic VO_2 thermochromic smart glass: A review on progress in solution processing, Nano Energy 1 (2012) 221-246.

[9] C. Wu, Y. Xie, Promising vanadium oxide and hydroxide nanostructures: from energy storage to energy saving, Energy Environ. Sci. 3 (2010) 1191-1206.

[10] P. Kiri, G. Hyett, R. Binions, Solid state thermochromic materials, Advanced Materials Letters 1 (2010) 86-105.

[11] X. Qian, N. Wang, Y. Li, J. Zhang, Z. Xu, Y. Long, Bioinspired Multifunctional Vanadium Dioxide: Improved Thermochromism and Hydrophobicity, Langmuir 30 (2014) 10766-10771.

[12] A. Taylor, I. Parkin, N. Noor, C. Tummeltshammer, M.S. Brown, I. Papakonstantinou, A bioinspired solution for spectrally selective thermochromic VO_2 coated intelligent glazing, Opt. Express 21 (2013) A750-A764.

[13] I.P. Parkin, T.D. Manning, Intelligent Thermochromic Windows, Journal of Chemical Education 83 (2006) 393-400.

[14] M. Zhou, J. Bao, M. Tao, R. Zhu, Y. Lin, X. Zhang, Y. Xie, Periodic porous thermochromic VO_2(M) films with enhanced visible transmittance, Chem. Commun. 49 (2013) 6021-6023.

[15] S. Ding, Z. Liu, D. Li, W. Zhao, Y. Wang, D. Wan, F. Huang, Tunable Assembly of Vanadium Dioxide Nanoparticles to Create Porous Film for Energy-Saving Applications, ACS Appl. Mater. Interfaces 5 (2013) 1630-1635.

[16] Y. Xu, W. Huang, Q. Shi, Y. Zhang, Y. Zhang, L. Song, Y. Zhang, Effects of porous nano-structure on the metal–insulator transition in VO_2 films, Appl. Surf. Sci. 259 (2012) 256-260.

[17] L. Kang, Y. Gao, H. Luo, Z. Chen, J. Du, Z. Zhang, Nanoporous thermochromic VO_2 films with low optical constants, enhanced luminous transmittance and thermochromic properties, ACS Appl. Mater. Interfaces 3 (2011) 135-138.

[18] J.T. Zhu, A.B. Huang, H.B. Ma, S.H. Bao, S.D. Ji, P. Jin, Solar-thermochromism of a hybrid film of VO_2 nanoparticles and CoII-Br-TMP complexes, RSC Adv. 6 (2016) 67396-67399.

[19] Z. Chen, Y. Gao, L. Kang, C. Cao, S. Chen, H. Luo, Fine crystalline VO_2 nanoparticles: synthesis, abnormal phase transition temperatures and excellent optical properties of a derived VO_2 nanocomposite foil, J. Mater. Chem. A 2 (2014) 2718-2727.

[20] J. Zhou, Y. Gao, X. Liu, Z. Chen, L. Dai, C. Cao, H. Luo, M. Kanahira, C. Sun, L. Yan, Mg-doped VO_2 nanoparticles: hydrothermal synthesis, enhanced visible transmittance and decreased metal-insulator transition temperature, Phys. Chem. Chem. Phys. 15 (2013) 7505-7511.

[21] Y.F. Gao, S.B. Wang, L.T. Kang, Z. Chen, J. Du, X.L. Liu, H.J. Luo, M. Kanehira, VO_2-Sb:SnO_2 composite thermochromic smart glass foil, Energy Environ. Sci. 5 (2012) 8234-8237.

[22] S.Y. Li, G.A. Niklasson, C.G. Granqvist, Nanothermochromics: Calculations for VO_2 nanoparticles in dielectric hosts show much improved luminous transmittance and solar energy transmittance modulation, J. Appl. Phys. 108 (2010) 063525.

[23] C. Liu, I. Balin, S. Magdassi, I. Abdulhalim, Y. Long, Vanadium dioxide nanogrid films for high transparency smart architectural window applications, Opt. Express 23 (2015) A124-A132.

[24] Q. Lu, C. Liu, N. Wang, S. Magdassi, D. Mandler, Y. Long, Periodical micro-patterned VO_2 thermochromic films by mesh printing, J. Mater. Chem. C (2016) DOI: 10.1039/C1036TC02694J.

[25] M.-H. Lee, J.-S. Cho, Better thermochromic glazing of windows with anti-reflection coating, Thin Solid Films 365 (2000) 5-6.

[26] C. Liu, N. Wang, Y. Long, Multifunctional overcoats on vanadium dioxide thermochromic thin films with enhanced luminous transmission and solar modulation, hydrophobicity and anti-oxidation, Appl. Surf. Sci. 283 (2013) 222-226.

[27] G.V. Jorgenson, J.C. Lee, Doped Vanadium Oxide For Optical Switching Films, Solar Energy Materials 14 (1986) 205-214.

[28] J.B. Goodenough, The Two Components of the Crystallographic Transition in VO_2, J. Solid State Chem. 3 (1971) 490-500.

[29] A. Romanyuk, R. Steiner, L. Marot, P. Oelhafen, Temperature-induced metal–semiconductor transition in W-doped VO_2 films studied by photoelectron spectroscopy, Sol. Energy Mater. Sol. Cells 91 (2007) 1831-1835.

[30] R. Binions, C. Piccirillo, I.P. Parkin, Tungsten doped vanadium dioxide thin films prepared by atmospheric pressure chemical vapour deposition from vanadyl acetylacetonate and tungsten hexachloride, Surf. Coat. Technol. 201 (2007) 9369-9372.

[31] N. Wang, M. Duchamp, C. Xue, R.E. Dunin-Borkowski, G. Liu, Y. Long, Single-Crystalline W-Doped VO_2 Nanobeams with Highly Reversible Electrical and Plasmonic Responses Near Room Temperature, Adv. Mater. Interfaces 3 (2016) 1600164.

[32] S.-Y. Li, N.R. Mlyuka, D. Primetzhofer, A. Hallén, G. Possnert, G.A. Niklasson, C.G. Granqvist, Bandgap widening in thermochromic Mg-doped VO_2 thin films: Quantitative data based on optical absorption, Appl. Phys. Lett. 103 (2013) 161907.

[33] J. Du, Y. Gao, H. Luo, Z. Zhang, L. Kang, Z. Chen, Formation and metal-to-insulator transition properties of VO_2–ZrV_2O_7 composite films by polymer-assisted deposition, Sol. Energy Mater. Sol. Cells 95 (2011) 1604-1609.

[34] N. Wang, M. Duchamp, R.E. Dunin-Borkowski, S. Liu, X. Zeng, X. Cao, Y. Long, Terbium-Doped VO_2 Thin Films: Reduced Phase Transition Temperature and Largely Enhanced Luminous Transmittance, Langmuir 32 (2016) 759-764.

[35] N. Wang, N.T. Chew Shun, M. Duchamp, R.E. Dunin-Borkowski, Z. Li, Y. Long, Effect of lanthanum doping on modulating the thermochromic properties of VO_2 thin films, RSC Adv. 6 (2016) 48455-48461.

[36] X. Cao, N. Wang, S. Magdassi, D. Mandler, Y. Long, Europium Doped Vanadium Dioxide Material: Reduced Phase Transition Temperature, Enhanced Luminous Transmittance and Solar Modulation, Sci. Adv. Mater. 6 (2014) 558-561.

[37] N. Wang, S. Liu, X.T. Zeng, S. Magdassi, Y. Long, Mg/W-codoped vanadium dioxide thin films with enhanced visible transmittance and low phase transition temperature, J. Mater. Chem. C 3 (2015) 6771-6777.

[38] G. Wyszecki, W.S. Stiles, Color Science: Concepts and Methods, Quantitative Data and Fomulae, Second ed., Wiley, New York, 2000.

[39] ASTM G173-03 Standard Tables of Reference Solar Spectral Irradiances: Direct Normal and Hemispherical on a 37° Tilted Surface, Annual Book of ASTM Standards American Society for Testing and Materials, Philadelphia, PA, USA, 2003.

[40] X. Cao, M.N. Thet, Y. Zhang, S.C. Joachim Loo, S. Magdassi, Q. Yan, Y. Long, Solution-based fabrication of VO_2(M) nanoparticles via lyophilisation, RSC Adv. 5 (2015) 25669-25675.

[41] J. Zhu, Y. Zhou, B. Wang, J. Zheng, S. Ji, H. Yao, H. Luo, P. Jin, Vanadium Dioxide Nanoparticle-based Thermochromic Smart Coating: High Luminous Transmittance, Excellent

Solar Regulation Efficiency, and Near Room Temperature Phase Transition, ACS Appl. Mater. Interfaces 7 (2015) 27796-27803.

[42] M.K. Dietrich, B.G. Kramm, M. Becker, B.K. Meyer, A. Polity, P.J. Klar, Influence of doping with alkaline earth metals on the optical properties of thermochromic VO_2, J. Appl. Phys. 117 (2015) 185301.

[43] W.Burkhar dt, T.Christmann, S.Franke, W.Kriegseis, D.Meister, B.K.Meyer, W.Niessner, D.Schalch, A.Scharmann, Tungsten and fluorine co-doping of VO_2 films, Thin Solid Films, 402 (2002) 226-231.

[44] K. Miyazaki, K. Shibuya, M. Suzuki, K. Sakai, J.-i. Fujita, A. Sawa, Chromium–niobium co-doped vanadium dioxide films: Large temperature coefficient of resistance and practically no thermal hysteresis of the metal–insulator transition, AIP Advances, 6 (2016) 055012.

[45] N.M. Ravindra, P. Ganapathy, J. Choi, Energy gap–refractive index relations in semiconductors – An overview, Infrared Physics & Technology, 50 (2007) 21-29.

[46] W. Zhang, K. Wang, L. Fan, L. Liu, P. Guo, C. Zou, J. Wang, H. Qian, K. Ibrahim, W. Yan, F. Xu, Z. Wu, Hole Carriers Doping Effect on the Metal–Insulator Transition of N-Incorporated Vanadium Dioxide Thin Films, J. Phys. Chem. C, 118 (2014) 12837-12844.